Multiray Photogrammetry and Dense Image Matching

NORBERT HAALA, Stuttgart

ABSTRACT

Dense matching of multiple overlapping aerial images can generate Digital Elevation Models at accuracies and densities, which could not be expected until recently. This increase in quality was mainly facilitated by the improved image quality as provided from digital airborne cameras and the development of suitable matching algorithms. Within the investigations presented in the paper, the Semi-Global Matching (SGM) stereo method is used for a pixel-wise matching in order to generate dense 3D point clouds. This matching is additionally combined with suitable filter algorithms, which exploit the redundancy of highly overlapping aerial images. By these means photogrammetric DEM generation is feasible at high quality. After a brief discussion of these algorithms the impact of different stereo configurations on the quality of the final outcome is evaluated. Within the investigations, special interest is paid to the combination of multiple stereo image pairs. As it will be demonstrated this can be used efficiently to increase the accuracy and reliability of the final matching results.

1. INTRODUCTION

For a considerable period, the acquisition of high quality Digital Elevation Models (DEM) was dominated by the use of airborne LiDAR. Meanwhile, automatic image based collection revived as a suitable alternative. This development was triggered by the increasing quality of digital airborne cameras as well as recent innovations in matching algorithms. Airborne imagery of good dynamic and signal-to-noise-ratio as available from digital aerial cameras is highly beneficial for automatic image matching. This is especially true for surfaces with relatively little surface texture. Consequently, the quality and accuracy of image based point transfer as basic observation for 3D surface reconstruction ameliorated considerably. Recent tests have already demonstrated the feasibility of image matching as a valid alternative to airborne LiDAR (Haala et. al., 2010) (Leberl et.al., 2010). Currently, commercial image matching software tools are still based on algorithms already established considerable time ago. Usually, they apply standard feature and intensity based matching for DEM raster generation. However, standard feature based approaches can suffer from regions of a rather limited number of matched points at areas of low image texture. On the other hand, during application of intensity based approaches the required minimum size of correlation windows frequently results in smoothing effects especially at object border and height discontinuities. These limitations of traditional approaches can be overcome by current algorithms aiming at a high resolution DEM computation. One example is the Semi-Global Matching (SGM) stereo method as proposed by (Hirschmüller, 2008), which provides a match for each image pixel. By these means a computation of dense 3D point clouds and DEM at surface resolutions similar to the ground sampling distance of the available imagery is feasible. The potential of the SGM algorithm was already demonstrated for different applications and data sets, including aerial images, satellite data or video sequences. This was our motivation to implement and use SGM for our evaluations on dense image matching.

In addition to suitable stereo matching algorithms, the quality of image based surface reconstruction mainly depends on the proper combination of multiple image information. Multi-view stereo reconstruction has a considerable tradition for close range applications in the computer vision community. There, parallax or disparity images are computed for different combinations of stereo image pairs from different camera viewpoints while the resulting so-called depth maps are merged in a second step to create a complete 3D model by triangle meshing. As also documented by the

performance evaluation of multi-view stereo reconstruction algorithms (Seitz et. al, 2006) a number of high-quality algorithms are available and the state-of-the-art still improves rapidly.
Similarly, airborne scenarios also benefit from multiple overlapping stereo pairs. This enables a reliable elimination of outliers and reduction of high frequency noise during DEM generation. Within our investigations, dense image matching was evaluated for multiple stereo configurations as available from highly overlapping image flights. Firstly, stereo image pairs with different base-to-height ratios were investigated to evaluate the general trade-of between good intersection geometry for large base-to-height ratios and simplified matching due to greater similarity of image content for short baselines. As it will be demonstrated, suitable integration of multiple overlapping images allows for consistency checks to elimination of erroneous matches and further improves completeness and geometric accuracy.
Within the paper the implement matching algorithm will be briefly introduced in the following section. Our accuracy investigations presented within section 3 are based on redundant 3D point measurement from multiple stereo pairs both at planar and a built-up test regions of higher geometric complexity. By these means the potential of multiray photogrammetry and dense image matching for high quality 3D data capture will be demonstrated.

2. DENSE IMAGE MATCHING

The image based measurement of 3D point clouds at densities corresponding to the resolution of the available stereo models presume matching results for each image pixel. In order to cope with the general ambiguity of such a per-pixel measurement, additional constraints such as the assumption of a smooth surface are usually introduced. Algorithms that globally minimize matching costs between corresponding pixels and the respective smoothness constraints are called global image matching. While they provide good results in terms of quality and resolution, they usually suffer from a high complexity, which results in rather low performance. However, this computational complexity can be reduced significantly by the Semi-Global Matching (SGM) stereo method. This approach, used for our investigations, approximates a global approach by minimizing matching costs, which are aggregated along a certain number of 1D path directions through the image. By these means, the pixel-wise SGM approach provides a dense point distribution, while the global approximation on paths enables a reasonable runtime on large imagery.

2.1. Semi-Global Matching

Our implementation of the SGM algorithm in large extent is similar to (Hirschmüller, 2008). The aim of this pixel-wise matching approach is to relate each pixel coordinate in the base image to its corresponding pixel coordinate in the match image. Each matching relation induces a matching cost. The sum of all costs defines the global matching cost which is assumed to be minimal for optimal pixel correspondences. Since the problem of minimizing global matching costs for 2D

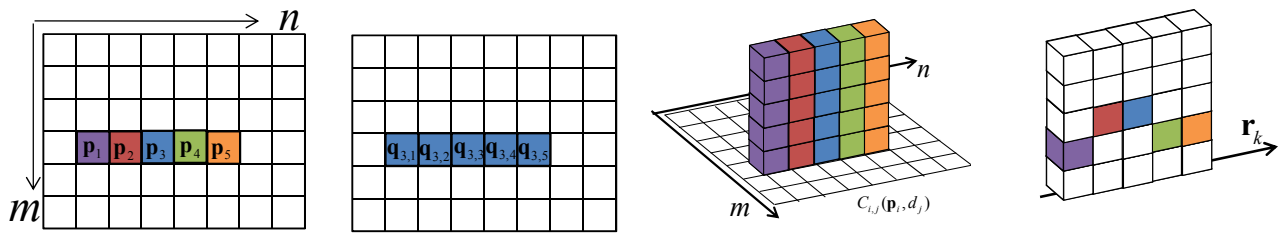

Figure 1: (a) Base image pixels $\mathbf{p}_{i=1\ldots5}$ (b) Potential correspondences $q_{3,j=1\ldots5}$ of $\mathbf{p}_3$ in the match image (c) Costs $c_{i=1..5,j=1\ldots5}$ assigned to the 3D cost cube (d) Minimal cost path along the image path r_k

images is known to be NP-hard, the idea of the SGM is to minimize an approximation of the global cost.

As it is visible in Figure 1, for each base image pixel $\mathbf{p}_i$ the matching costs $c_{i,j}(\mathbf{p}_i,\mathbf{q}_i)$ for a set of D potential correspondences $\mathbf{q}_{i,j=1,\ldots,D}$ in the match image are calculated. Within all tests the Mutual Information (MI) matching cost was used as a measure for the similarity of two images. Since epipolar lines are computed from results of the preceding bundle block adjustment, the search for potential corresponding pixels can be limited to $\mathbf{q}_{i,j}=\mathbf{e}(\mathbf{p}_i,d_i)$, with the disparity or parallax d_i specifying the actual position on $\mathbf{e}_i$. The minimal costs $c_{i,j}(\mathbf{p}_i,\mathbf{q}_i)$ of the set of potential correspondences then define a first estimation of the disparity. Unfortunately, these cost minima often are not distinctive and result in wrong parallax estimations. This problem can be solved by cost aggregation. For this purpose a N×M×D cost structure or 3D cost cube containing the costs $c_{i,j}(\mathbf{p}_i,d_i)$ is assembled. It contains the matching costs of N×M base image pixels and their D potential correspondences in the match image. The final aggregated matching cost $s(\mathbf{p}_i,d_i)$ of a base image pixel and its potential correspondence is then derived by summation of minimal costs along 16 image paths. During cost aggregation, penalty terms are introduced which potentially smooth these cost paths, while the possibility of non-continuous paths is still maintained. The final correspondence or parallax is then defined by the minimum of the aggregated matching cost $s(\mathbf{p}_i,d_i)$ while sub-pixel disparities are estimated by quadratic curve fitting.

Figure 2: Stereo pair with corresponding parallax image

Figure 2 depicts an exemplary result of this matching process. Base and match image after normalization by transformation to epipolar geometry are given on the left and middle, respectively. The parallax image from SGM, which provides the disparity for each pixel in the base image with respect to the match image is shown on the right. Within this disparity image black areas are visible. These correspond to apparently wrong parallaxes of the core SGM process which were eliminated by a filter algorithm. This filter was realized by a simple consistency check with changed roles of base and match images during matching. Only disparity estimations consistent to this forward-backward matching are then considered as valid. Additional erroneous disparity estimations are removed by filtering the disparity images with conservative smoothing (Jain, 1986) and a subsequent occlusion check (Hirschmüller, 2008).

2.2. Object point triangulation

After parallax estimation object point coordinates are computed by spatial intersection. For this purpose the corresponding pixels in the stereo pair as defined by the disparity images are used. Within our implementation, the spatial intersection method described by (Hartley & Zisserman, 2004) is implemented. There the transformations $\mathbf{x} = (x, y, 1)^{\mathbf{T}} = \mathbf{PX}$ and $\mathbf{x}' = (x', y', 1) = \mathbf{P}'\mathbf{X}$ of

object points $\mathbf{X}$ into the two image planes are given by the projection matrices $\mathbf{P}$ and $\mathbf{P}'$.These matrices represent the respective exterior and interior orientations from bundle block adjustment. The projections are reformulated to $\mathbf{x} \times (\mathbf{PX}) = \mathbf{0}$ and $\mathbf{x}' \times (\mathbf{P}'\mathbf{X}) = \mathbf{0}$ .These equations are formulated explicitly in (1.1) and (1.2), respectively.

$$\begin{aligned} x(\mathbf{p}^{3T}\mathbf{X}) - (\mathbf{p}^{1T}\mathbf{X}) &= 0 \\ y(\mathbf{p}^{3T}\mathbf{X}) - (\mathbf{p}^{2T}\mathbf{X}) &= 0 \\ x(\mathbf{p}^{2T}\mathbf{X}) - y(\mathbf{p}^{1T}\mathbf{X}) &= 0 \end{aligned} \quad (1.1)$$

$$\begin{aligned} x'(\mathbf{p}'^{3T}\mathbf{X}) - (\mathbf{p}'^{1T}\mathbf{X}) &= 0 \\ y'(\mathbf{p}'^{3T}\mathbf{X}) - (\mathbf{p}'^{2T}\mathbf{X}) &= 0 \\ x'(\mathbf{p}'^{2T}\mathbf{X}) - y'(\mathbf{p}'^{1T}\mathbf{X}) &= 0 \end{aligned} \quad (1.2)$$

$$\mathbf{A} = \begin{pmatrix} x\mathbf{p}^{3T} - \mathbf{p}^{1T} \\ y\mathbf{p}^{3T} - \mathbf{p}^{2T} \\ x'\mathbf{p}^{3T} - \mathbf{p}^{1T} \\ y'\mathbf{p}^{3T} - \mathbf{p}^{2T} \end{pmatrix} \quad (1.3)$$

Within equations (1.1) and (1.2) $\mathbf{p}^{iT}$ denotes the i'th row in the 3×4 camera matrix. Using these equations a linear system of the form $\mathbf{AX} = \mathbf{0}$ can be composed with $\mathbf{A}$ given in equation (1.3). This system is then solved using an SVD to compute the coordinates of object point $\mathbf{X}$. Such a resulting 3D point cloud is depicted in .

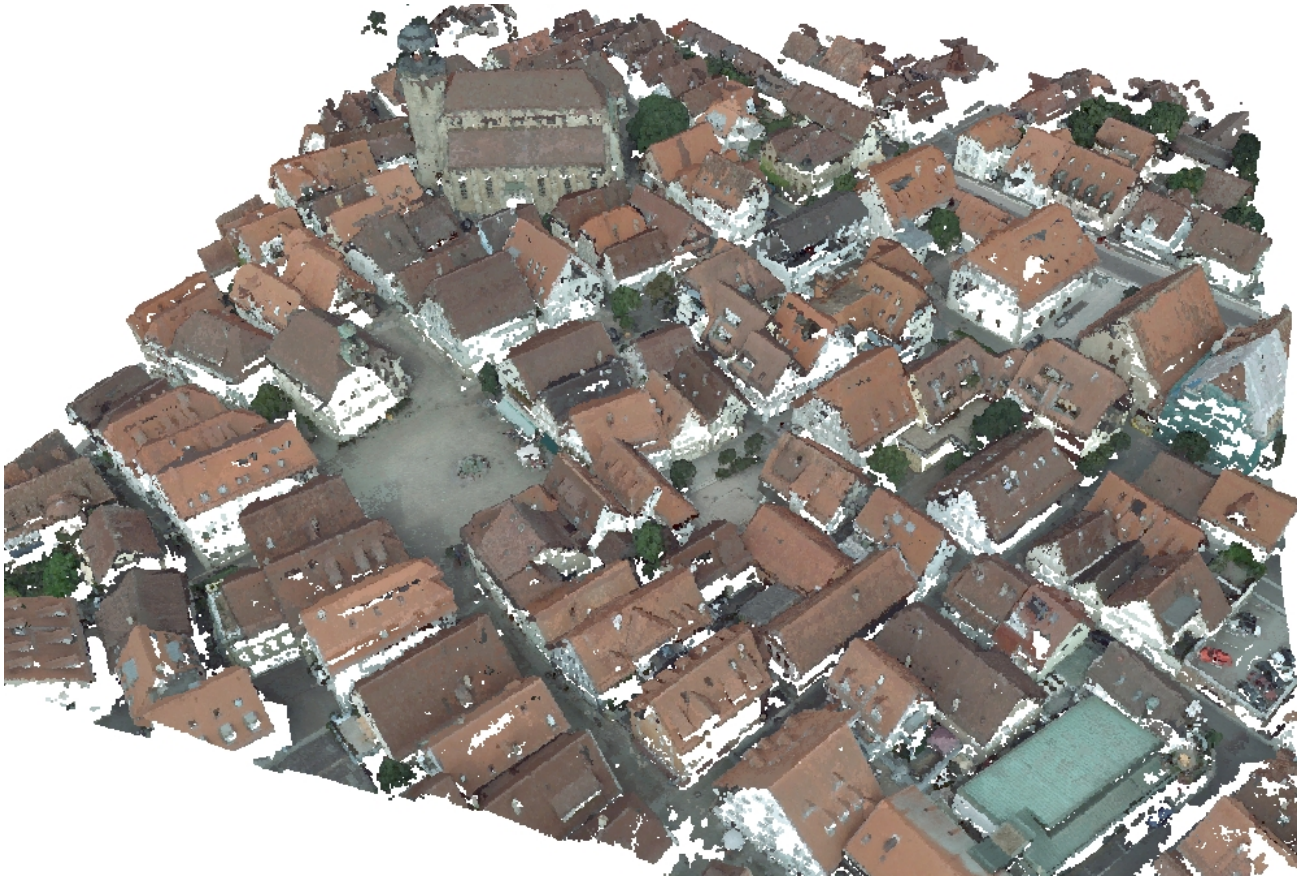

Figure 3: Point cloud from dense matching of two stereo pairs

2.3. Combination of multi strip measurements

The per-pixel disparity measurements as provided from SGM already generate dense 3D point clouds at a resolution of the available aerial imagery. However, a considerable amount of occluded regions can occur especially within build-up areas. For this reason, applications like true-ortho image generation suffering from the same problem, increase the side overlap of the utilized aerial image flights from the traditional 20% to an amount of 60%. Thus each object point is visible in at least two image strips and no-data regions can be avoided.

Figure 4: Stereo pair from additional flight line with corresponding parallax image

As it is demonstrated in Figure 4, this enables parallax measurements for the same area already depicted in Figure 2 using images of the adjacent strip. By these means an additional point cloud is generated, which is then used to lessen occluded areas. The 3D point cloud depicted in was generated by a simply putting together these two point clouds from two different stereo pairs. This already provides data sets at considerable density and completeness. However, the redundancy of such multiple overlaps can be used even more efficiently for accuracy analysis and suitable filter operations during multiple stereo matching as demonstrated in the following section.

3. MULTIPLE STEREO MATCHING

Traditional airborne photogrammetry used to limit the cost for film material and the effort for manual stereo measurement by minimizing the number of images to be collected and evaluated. This was realized by the typical 60% forward and 20% sideward overlap of image blocks. By these means the availability of one stereo image pair for each object point and a block geometry of suitable geometry could be guaranteed. Meanwhile, extra costs for additional image acquisition can almost be neglected by using digital photogrammetric cameras. Thus, 80% forward overlap can be easily generated. In contrast, the increase of available sidelap requires additional flight lines. This will rise the costs since more flying time is required. However, flights with 60% sidelap are already realized for applications like true orthophoto generation (Braun, 1996). Especially in dense urban areas, multiple overlapping images are required for this application to fill image regions obscured due to relief displacement.
Overlaps of 80% along track and 60% cross track will result in at least 10 images per object point. This is a considerable increase of redundancy compared to two image rays as available for image based surface reconstruction from traditional photogrammetric blocks. These multiple image rays can then be used to eliminate of mismatches by suitable filter processes and increase the accuracy of image based 3D point cloud generation.

3.1. Test data set

In order to investigate the benefits of multiray photogrammetry, a test flight with an approximate overlap of 80% in flight direction and 70% orthogonal to the flight direction was evaluated. The aerial imagery was captured by Vexcel's UltraCamXp in the test area Gleisdorf at a height above terrain of 1600m with a GSD of approximately 10cm. Figure 5 shows a test area selected from this block which is used in the following investigations. It includes several potentially problematic regions for image matching marked by solid rectangles. These areas contain low texture (yellow), varying shadows due illumination changes (purple), periodic patterns (red and green), vegetation of varying appearance in different images (orange) and smaller structures as cars (blue). Furthermore, the dashed rectangle defines a planar area which is especially suitable for accuracy investigations.

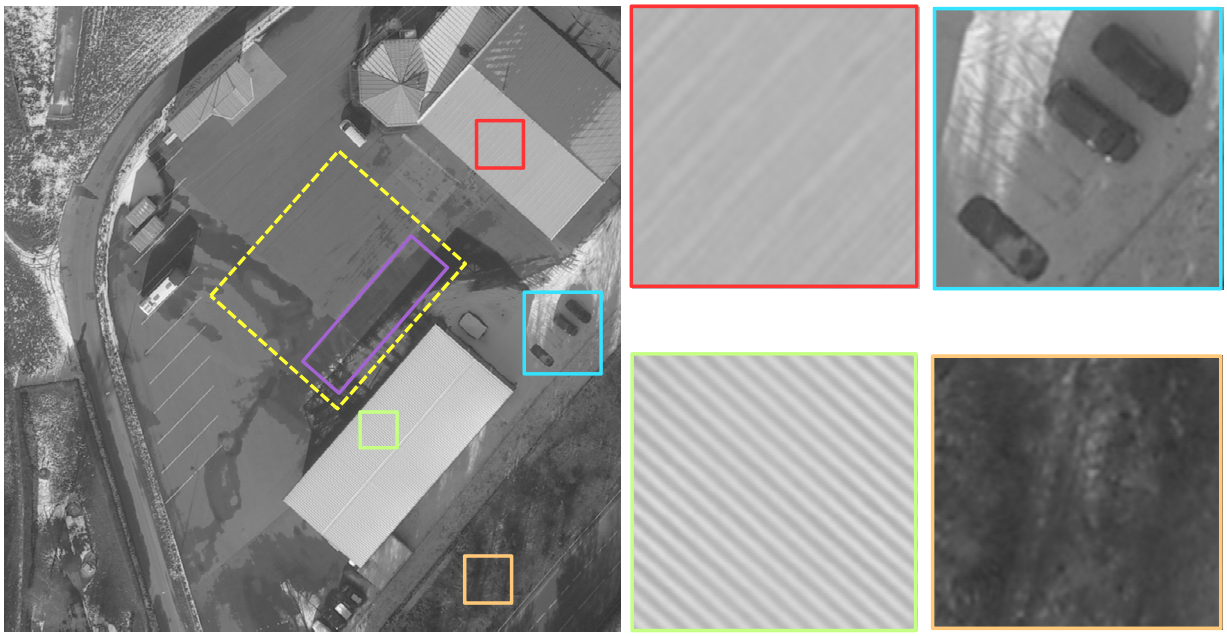

Figure 5: Test area with rectangles defining problematic areas for image matching

3.2. Evaluation of stereo matching accuracy

Multiple overlaps can be used to generate stereo image pairs at varying base-to-height ratios. The influence of such variations on the accuracy and reliability of SGM-based point measurement was evaluated by a pair-wise matching of five images from the same flight strip. For this purpose one image of the test area was treated as the base image and then matched against the following images of the same strip.

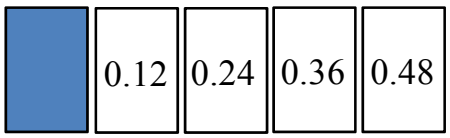

Figure 6: Base-to-height ratios for investigated stereo configurations

This configuration is depicted in Figure 6. The base image is represented by the blue rectangle. The numbers in the remaining rectangles then represent the base-to-height ratios for the neighbor images from the same image strip. These images were used as match images during generation of stereo image pairs. The rectangular shape of the image footprints is due to the image size of 17,310 pixel across track and 11,310 along track for the UltraCamXp used in our investigations. As it is visible

in Figure 6, the base-to-height ratio is 0.125 for proximate images. Accordingly, the largest base-to-height ratio for a stereo image pair was 0.48.

The accuracy of point clouds from SGM for the different stereo image combinations was first investigated for the 40x30m^2 planar region marked by the yellow rectangle in Figure 5. A 3rd order polynomial was fit to the generated 3D point cloud. The respective residuals to that surface could then be used to measure the corresponding point accuracies. These are given in Table 1. The first row presents the base-to-height ratios for the investigated stereo pairs according to Figure 6. The resulting point accuracies from surface approximation are given in the second row. To determine these accuracies, mismatches were eliminated in a first step. For this purpose 3D points with a deviation larger than the standard deviation of 3σ from the estimation of the 3rd order polynomial were marked as outliers. The error σ_{3mv} then gives the standard deviation of the remaining points to this approximated surface. The amount of valid matches with respect to all matched points n_{Points}[%] is then given in the third row.

The accuracy σ_{3mv}[cm] of 3D points in object space is influenced by the respective matching accuracy as well as the geometric configuration during spatial intersection. This configuration is mainly defined from the respective base-to-height ratio. Thus, the matching accuracy σ_{3mv}[pix] within image space can be derived by simple error propagation from the 3D point accuracy for the respective stereo configurations as given in the second row. These accuracies are given in the fourth row of the table. Alternatively, matching accuracies can be determined from the differences between forward and backward matching. This approach is much more flexible, since no comparison to a reference surface is required. Within Table 1, these values are given in the fifth row. These values are similar to the accuracies from error propagation, which demonstrates the validity of this measure for error estimation.

Base-to-height ratios	0.12	0.24	0.36	0.48
Point accuracies in object space σ_{3mv}[cm]	11.09	10.43	7.66	5.75
Ratio of successfully matched points n_{Points}[%]	98.99	91.97	89.09	86.63
Matching accuracy from error propagation σ_{3mv}[pix]	0.12	0.23	0.25	0.25
Accuracy from forward-backward matching σ_{3mv}[pix]	0.15	0.20	0.23	0.23

Table 1: Matching quality for different stereo configurations

The results of matching quality for different stereo configuration in Table 1 show, that the matching accuracy in image space decreases for larger baselines from 0.12pix to 0.25pix. Apparently, SGM is slightly more sensitive to viewpoint changes and radiometric differences compared to standard matching approaches used within aerial triangulation. Our bundle block adjustment resulted in tie point accuracies of approximately 0.1pix for all measures. However, it must be kept in mind that during automatic aerial triangulation (AAT) tie points are provided by a combination of feature and intensity based matching. Thus, AAT selects image points especially suitable for matching in a pre-processing step, while SGM provides a match for each image pixel. Table 1 also shows, that despite of the decreasing matching accuracy for larger baselines, the corresponding point accuracies in object space are improving. Thus, less accurate matching results can be compensated by beneficial geometric configurations. However, shorter base-to-height ratios are preferable with respect to the number of successful matches. This number decreases from 98.99% for the smallest base-to-height ratio to 86.63% for the largest one.

3.3. Improvements from multiple stereo image configurations

Despite the fact that differences between forward-backward matching can provide a suitable estimate of matching quality, an evaluation based on 3D point accuracy usually is much more reliable. For this purpose a planar test area was used in the previous investigations. However, multiple matches provide a much very flexible tool for the evaluation of point accuracies at arbitrary areas. Multiple matches are realized by defining the central image for an area of interest as the base image, which is then matched against the surrounding images. Thus, corresponding measurements across multiple match images are related by a pixel coordinates $\mathbf{x}_b^i$ in the base image and the corresponding pixel coordinates $\mathbf{x}_m^i$ in the respective match images. Consequently, they can be assumed to represent the same object point $\mathbf{X}$. In that scenario the matrix $\mathbf{A}$ in equation (1.3) changes to

$$\mathbf{A} = \begin{pmatrix} x_b\mathbf{p}_b^{3\mathbf{T}} - \mathbf{p}_b^{1\mathbf{T}} \\ y_b\mathbf{p}_b^{3\mathbf{T}} - \mathbf{p}_b^{2\mathbf{T}} \\ x_m^1\mathbf{p}_m^{1,3\mathbf{T}} - \mathbf{p}_m^{1,1\mathbf{T}} \\ y_m^1\mathbf{p}_m^{1,3\mathbf{T}} - \mathbf{p}_m^{1,2\mathbf{T}} \\ x_m^2\mathbf{p}_m^{2,3\mathbf{T}} - \mathbf{p}_m^{2,1\mathbf{T}} \\ \cdots \end{pmatrix} \quad (1.4)$$

Now it contains two rows for the base image pixel $\mathbf{x}_b$ and two rows for each of the match images $\mathbf{x}_m^i$. Each additional stereo model generated by mapping an additional match image against the base image will increase the number of image rays to be intersected for object point determination by one. For n stereo pairs depicting an identical object point, n+1 observations will be available.
Object point triangulation is then again realized by solving the system $\mathbf{AX} = \mathbf{0}$. By these means, in principle image rays as defined by the corresponding image coordinates are intersected. However, both remaining errors from aerial triangulation and disparity measurement by SGM will result in small deviations of these image rays from the estimated object point. Thus, the least-squares-solution of the linear system $\mathbf{AX} = \mathbf{0}$ gives a good measure for the respective point accuracy. This accuracy is derived from the diagonal elements δ_X^2, δ_Y^2 and δ_z^2 of the covariance matrix $\sigma^2(\mathbf{A}^\mathbf{T}\mathbf{A})^{-1}$ with the value $\sigma^2 = \frac{\mathbf{v}^\mathbf{T}\mathbf{v}}{m-u}$ computed from residuals $v_i = \hat{\mathbf{x}}_m^i - \mathbf{x}_m^i$ of the respective pixel observations. For this purpose the estimated object point is reprojected into all the images by $\hat{\mathbf{x}}_m^i = \mathbf{P}_m^i\hat{\mathbf{X}}$. Since the least squares solution provides for the accuracy of the estimated object coordinates, this can be used to eliminate erroneous matches and to evaluate the accuracy of the remaining point cloud. In our investigations, this was first realized for different configurations of two stereo pairs generated from three images.

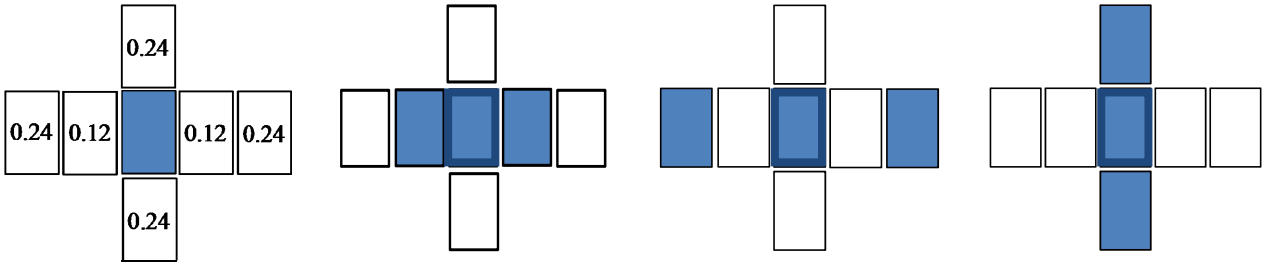

Figure 7: Base-to-height ratios and configurations for multi-stereo-matching

The blue rectangle with the bold outline in Figure 7 represents the central base image, which is transferred to two match images again depicted in blue. As it is visible, for stereo measurement configuration 1 uses the direct neighbors in flight direction. In configuration 2 the base-length of the respective stereo pairs increases by a factor of two since the second next images are used. Configuration 3 then generates stereo pairs from different image strips. As it is visible in the first column of Figure 7 these stereo pairs feature the same base-to-height ratios as the pairs in flight direction of configuration 2. Similar to the investigations presented in section 3.2. outliers are removed using a threshold of 3σ computed from all 3D point measurements. However, since this standard deviation is provided from the redundancy of two stereo image pairs using equation (1.4), no assumption on underlying object geometry is required. In contrast to the investigations in the section 3.2. matching is not restricted to the planar region. Thus, vertical point accuracies δ_Z and the ratio of successfully matched points can be determined for arbitrary areas.

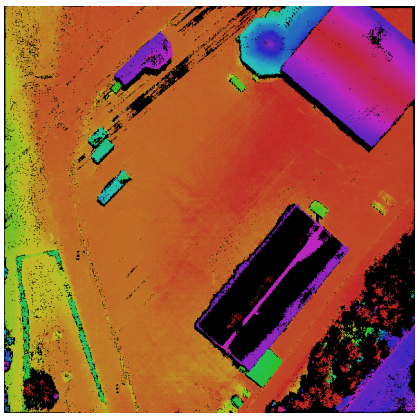

Config. 1 δ_Z=4.27cm n_{Points}=81.4%

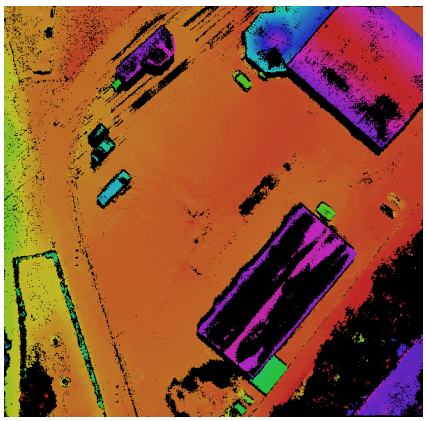

Config. 2 δ_Z=1.94cm n_{Points}=72.8%

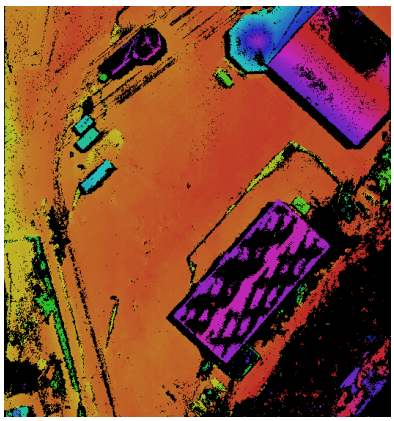

Config. 3 δ_Z=1.91cm n_{Points}=60.1%

Table 2: Matching results for configurations 1 – 3

The matching results for the different configurations are given in Table 2. The distribution of the eliminated outliers within the test area is visible in the color coded point clouds. Areas with no valid point measurements occur as black regions. Similar to the investigations in section 3.2. , the number of successfully matched points decreases if the base-to-height-ratio is increased. For the combination of the stereo pairs with base-to-height-ratio of 0.12 in configuration 1, successful matches were generated for 81.4% of all points. This corresponds to a point density of 86pts/m^2 for the available imagery. This value decreases to 72.8% for the base-to-height-ratio of 0.25 in configuration 2.

Compared to percentages of successfully matched points in Table 1 the values are lower in Table 2. However, for the measurements in Table 1 a successful point measurement requires a valid match in one stereo pair, while for Table 2 a point has to be determined from valid matches in two stereo pairs. Furthermore, measurements in Table 1 are restricted to the planar region, while for Table 2 the complete test area is examined, which includes problematic areas for image matching. Table 2 gives an average vertical accuracy δ_Z=4.27cm for points from configuration 1. In contrast, δ_Z is better than 2cm for configurations 2 and 3 due to the improved geometric configuration. It must be kept in mind that these accuracies just represent an internal geometry from the intersection of image rays. However, even if the additional error from bundle block adjustment is considered, the geometric quality of the generated point clouds is remarkable.

The distribution of no point areas in Table 2 show problems for all configurations at the repetitive pattern of the building roof marked by the green rectangle in Figure 5. For the larger base-to-height-ratio of configuration 2 and 3 additional problems occur especially at the bushes and trees marked by the orange rectangle in Figure 5. Such objects are difficult for stereo matching since their

appearance in the aerial images is especially sensitive to viewpoint changes. The number of matched points is even lower for configuration 3, which features the same base-to-height-ratio as configuration 2, but uses images from different image strips. There the larger time differences between times of exposure results in shadow movement, which again aggravates the matching process.

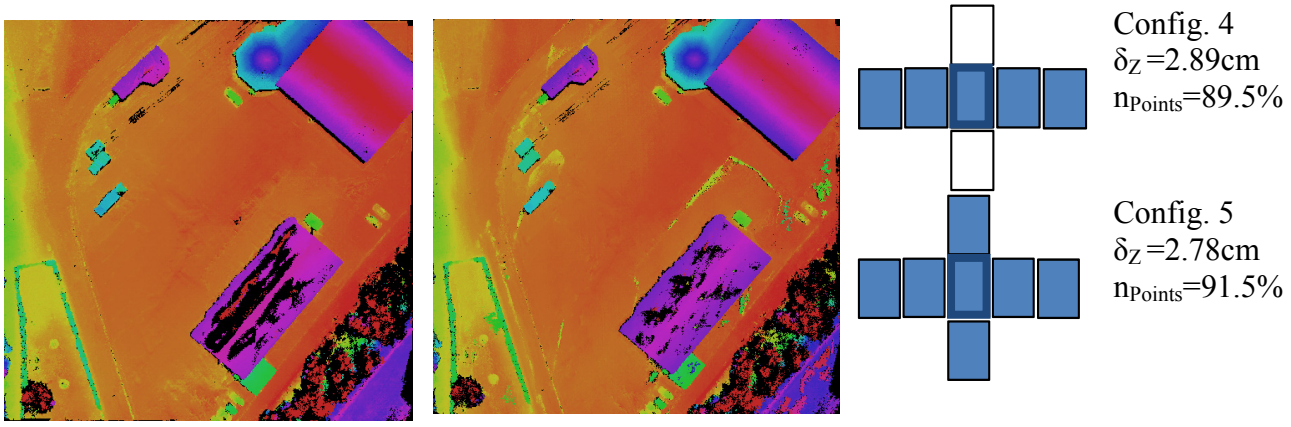

Table 3: Matching results for configuration 4 and 5 with for four (left) and six image pairs (right)

A further increase of both accuracy and density or completeness of 3D point clouds is feasible if multi stereo matching is extended to even more image pairs. This is demonstrated in Table 3, which displays results of four and six image pairs. For the left example, which defines configuration 4, five images of one strip are used to form four stereo image pairs. The second example derined as configuration 5 additionally includes two neighbor images from the upper and lower image strip to generate two more stereo pairs. Compared to configuration 2 and 3 in Table 1, the vertical errors δ_Z slightly increases after the additional imagery is included. This holds true for both configuration 4 and 5. This is due to the fact that an increasing number of image rays for point determination gives a better evidence on remaining errors in image orientation from bundle block adjustment. However, the use of additional stereo pairs considerably increases the percentage of successfully measured 3D points. These values increase to 89.5% and 91.5% for configuration 4 and 5, respectively. Although the increase of successfully matched points between configurations 4 and 5 is rather low, the additional computation is still useful. The two additional stereo pairs in configuration 5 provide points for viewpoints as provided from images of different strips. Thus they enhance the point clouds mainly by previously covered areas, as facades.

4. CONCLUSIONS

Within our investigations SGM proved to be a very efficient tool for very detailed, reliable and accurate image based 3D surface reconstruction. Even more important, the redundancy as available from the combination of stereo matches from different image pairs allows a very efficient accuracy analysis. This enables an efficient elimination of erroneous matches, which results in a considerable reliability matched points at vertical accuracies well at the sub-pixel level. Furthermore, multiple viewpoints also provide a good coverage at complex urban areas, which further increases the enormous number of potential applications of multi-ray photogrammetry from dense image matching.

5. REFERENCES

Braun, J. (2003): Aspects on True-Orthophoto Production. Photogrammetric Week '03, Herbert Wichmann Verlag, Heidelberg.

Leberl, F., Irschara, A., Pock, T., Meixner, P., Gruber, M., Scholz, S., Wiechert, A. (2010): Point Clouds: Lidar versus 3D Vision. Photogrammetric Engineering and Remote Sensing, Vol. 76, No. 10, pp 1123-1134.

Haala, N., Hastedt, H., Wolff, K., Ressl, C. & Baltrusch, S. (2010): Digital Photogrammetric Camera Evaluation – Generation of Digital Elevation Models. Photogrammetrie – Fernerkundung – Geoinformation (PFG). No. 2, pp. 99-115.

Hartley R.I. & Zisserman A. (2004): Multiple View Geometry in Computer Vision. Cambridge University Press, Chap. 12.

Hirschmüller, H. (2008): Stereo Processing by Semi-Global Matching and Mutual Information. IEEE Transactions on Pattern Analysis and Machine Intelligence, 30 (2), pp. 328-341.

Jain, A. (1986): Fundamentals of Digital Image Processing. Prentice-Hall, Chap. 7.

Seitz, S., Curless, B., Diebel, J., Scharstein, D. & Szeliski, R. (2006): A Comparison and Evaluation of Multi-View Stereo Reconstruction Algorithms. IEEE Computer Society Conference on Computer Vision and Pattern Recognition (CVPR'2006).